Title	Asymmetric shift of exchange bias loop in Ni-Ni(OH)2 core-shell nanoparticles
Author(s)	Maity, Tuhin; Roy, Saibal
Publication date	2018-05-24
Original citation	Maity, T. and Roy, S. (2018) 'Asymmetric shift of exchange bias loop in Ni-Ni(OH)2 core-shell nanoparticles', Journal of Magnetism and Magnetic Materials. doi:10.1016/j.jmmm.2018.05.064
Type of publication	Article (peer-reviewed)
Link to publisher's version	http://dx.doi.org/10.1016/j.jmmm.2018.05.064 Access to the full text of the published version may require a subscription.
Rights	© 2018, Elsevier B.V. All rights reserved. This manuscript version is made available under the CC-BY-NC-ND 4.0 license. https://creativecommons.org/licenses/by-nc-nd/4.0/
Embargo information	Access to this article is restricted until 24 months after publication by request of the publisher.
Embargo lift date	2020-05-24
Item downloaded from	http://hdl.handle.net/10468/6245

University College Cork, Ireland
Coláiste na hOllscoile Corcaigh

Accepted Manuscript

Asymmetric shift of exchange bias loop in Ni-Ni(OH)$_2$ core-shell nanoparticles

Tuhin Maity, Saibal Roy

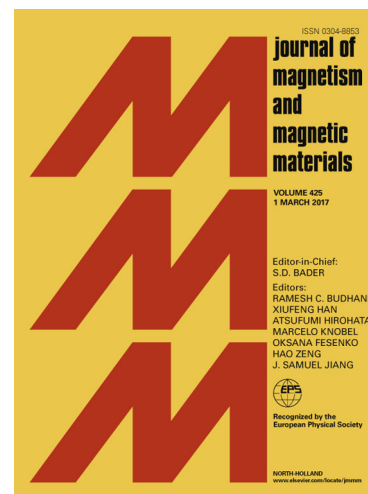Please cite this article as: T. Maity, S. Roy, Asymmetric shift of exchange bias loop in Ni-Ni(OH)$_2$ core-shell nanoparticles, *Journal of Magnetism and Magnetic Materials* (2018), doi: https://doi.org/10.1016/j.jmmm.2018.05.064

Asymmetric shift of exchange bias loop in Ni-Ni(OH)$_2$ core-shell nanoparticles

Tuhin Maity[1,3] and Saibal Roy[1,2,]*

[1]Tyndall National Institute, Lee Maltings, Dyke Parade, Cork, Ireland
[2] Department of Physics, University College Cork (UCC), Ireland

*Correspondence to: saibal.roy@tyndall.ie

ABSTRACT: We report the observation of the asymmetric shift of exchange bias loop in Ni-Ni(OH)$_2$ core-shell nanoparticles where the average size of the ferromagnetic (FM) Ni nanoparticles is ~30 nm and the thickness of antiferromagnetic (AFM) Ni(OH)$_2$ shell is ~5nm. The exchange bias (EB) found below Néel temperature (T_N~22 K) of Ni(OH)$_2$ is path dependent, while the coercivity (H_C) increases and decreases for positive and negative bias field respectively. In the present case, we found that the inversion symmetry of hysteresis loop is broken and the shift in EB loop is only observed in descending part of the hysteresis loop, which is conspicuous. We demonstrate that the asymmetric shift of EBs in these core-shell nanoparticles is due to the presence of frustrated super spin glass (SSG) at the interface which influences the reversal mechanism of the hysteresis loop. It is argued that the net interface moment from the SSG at the interface of core-shell nanoparticles sets a unidirectional anisotropy after field cooling, which is thought to be the origin of this path dependency of the EB and observed via descending part of the hysteresis loop, ushering potential for novel spin based applications.

1. Introduction

Interest in ferromagnetic (FM) nanoparticles has increased manifold in the past few years catalysed by virtue of their potential applications in rapidly expanding areas, ranging from ultrahigh density recording media to medicine [1-4]. With the decrease of particle size of the FM nanoparticles, the magnetic anisotropy energy becomes comparable to the thermal energy and the nanoparticles lose their stable magnetic order with random flipping of magnetic moments which leads them to become superparamagnetic. Hence the demand for further reduction of particle size faced a limitation known as 'superparamagnetic limit' [5-9]. Later it was observed that, nanoparticles with the ferromagnetic (FM) core-antiferromagnetic (AFM) shell morphology can overcome the limit where an extra source of anisotropy i.e. exchange anisotropy [9] is generated at the interface leading to the stabilization of magnetization. Two characteristic features, horizontal shift of the hysteresis loop in the direction opposite to the cooling field and an increase in the H_C relative to the bare FM particle are often observed. In most FM-AFM core-shell nanoparticles, the exchange bias (EB) arises from the pinning of magnetic moments at the interface between the two materials [10-12]. Despite the technological importance of EB especially in core-shell nanoparticles where the high degree of disorder is found in coupling between the surface-spins of the shell and core, the physical origin of different EB phenomena is still not fully understood [12-15]. Despite its original invention in nanoparticle systems, in the last few decades, the majority of research on EB has been conducted on flat interfaces in multi-layered thin films due to its important application in magnetic recording technologies [11, 16]. Recently EB in bi-magnetic nanoparticles has

regained its interest due to its potential application particularly in future single nanoparticle data storage systems, hyperthermia treatment of tumours, etc. [17].

Though the loop shift in exchange biased system has been extensively studied, qualitative and quantitative understanding of the change in coercivity in an exchange-bias system is still lacking. Some intrinsic correlations between exchange bias field (H_E) and H_C provide the important clue as to the microscopic origin of EB. However, precise and well controlled experimental investigations of H_C and its effect on H_E are rare particularly in nanoparticulate systems. A common feature in core-shell nanoparticle systems which exhibits EB is a vertical shift of hysteresis loop along the magnetization axis along with asymmetry in the remanent magnetization in ascending and descending parts of the hysteresis loop [18]. The EB in nanoparticles is attributed to uncompensated spins at the interface of superparamagnetic core – antiferromagnetic shell. Such uncompensated surface spins often behave as super-spin-glass (SSG) and influence the EB coupling [15, 19 - 22]. Monte Carlo simulations show that the net magnetization of the interfacial spins is responsible for the asymmetry in EB [22, 23]. On the other hand, several reports on asymmetric EB in the field axis, where the EB shift for positive and negative bias field is asymmetric, attract further interest for potential application in tunnel junction based magnetic recording, sensors, actuators, and other spintronic devices. [24-26] Thus understanding of asymmetric shift of coercive field for descending and ascending part of the hysteresis loop is crucial.

Here, we report asymmetric EB in Ni-Ni(OH)$_2$ core-shell nanoparticles below Néel temperature ($T_N \sim 22K$) of Ni(OH)$_2$ and the blocking temperature ($T_B \sim 60K$) of Ni nanoparticles. The H_C increases and decreases due to positive and negative bias field respectively which leads to asymmetric EB. Further, it is observed that the asymmetric loop shift for positive and negative bias field comes only from the asymmetric shift in descending part of the hysteresis loop due to the presence of SSG spin morphology at the interface between the core and the shell. The dependence of EB and coercivity on a cooling field can be explained by a model where the interface spin is modified and frustrated by the applied field while cooling. A unidirectional anisotropy at the interface thus set under field turns out to be in the negative direction which gives rise to the asymmetric EB [27-31].

2. Experimental procedure

Ni-Ni(OH)$_2$ core-shell nanoparticles were chemically synthesized using an aqueous mixture of 1×10^{-3}M Ni(NO$_3$)$_2$.6H$_2$O, 1×10^{-4}M oleic acid and 1×10^{-2}M (sodium dodecyl sulphate) SDS. The solutions were reduced using 0.035 g of NaBH$_4$ in solid form. The solutions were then centrifuged to separate the pellets. After that, the samples were fully dried in an air environment to produce a dry powdered sample. Details of the particle synthesis and structural analysis have previously been reported [30]. From detail HRTEM analysis we found that the nanoparticles have large size distribution ranging from ~25 nm to ~45 nm and there is always a possibility for the particles to agglomerate. The average Ni particle size is ~30 nm and the Ni(OH)$_2$ shell thickness is ~5 nm around the Ni core [Figure 1a]. Due to the presence of antiferromagnetic Ni(OH)$_2$ shell the superparamagnetic nature of Ni core remains stable even if nanoparticles agglomerate. A schematic representation of core (FM)-shell (AFM) structure of nanoparticles and their relative orientations of the atomic moments at different stages of hysteresis loop tracing are shown in Figure 1b.

The magnetic measurements across temperature range 2–350 K have been carried out in a SQUID magnetometer (MPMS XL5, Quantum Design) under a maximum field H_m of 50 kOe. All precautions were taken to ensure that there is no trapped flux both in the superconducting coil of SQUID magnetometer and in the sample. The superconducting coils of the SQUID were warmed to room temperature and also discharged from high field (50 kOe) in oscillation mode to remove any trapped flux. A well-designed protocol was followed to demagnetize the sample before starting each measurement [31]. The zero-field-cooled and field cooled (ZFC and FC) measurement was done to identify the phase transition of the materials. 10 Oe field was applied during the measurements (Figure 2a). Further to probe the characteristics of the system with different magnetic phases a series of temperature dependent AC susceptibility χ (T) measurements were carried out at 1, 10, 100 and 1000 Hz frequencies. The conventional exchange bias (CEB) measurements across 2-300 K after cooling down the sample from 350 K under ±50 kOe bias field are shown in Figure 2b & c where the hysteresis loops were measured by positive (+50 kOe $\rightarrow$ 0 $\rightarrow$ −50 kOe $\rightarrow$ 0 $\rightarrow$ +50 kOe) and negative (−50 kOe $\rightarrow$ 0 $\rightarrow$ +50 kOe $\rightarrow$ 0 $\rightarrow$ −50 kOe) loop tracing protocols respectively while cooling down with positive (+50 kOe) and negative field (-50 kOe) respectively. The H_E is given by $(H_{C2}+H_{C1})/2$ while the H_C is given by $(H_{C2}-H_{C1})/2$; H_{C1} and H_{C2} are the fields (signs are included) corresponding to the points in descending and ascending branches of the hysteresis loop at which the magnetization reaches zero. The exchange bias (H_E), remanence magnetization (M_R), coercivity (H_C) and saturation field (H_S : where both ascending and descending loops coincide) are plotted as a function of temperature (Figure 2b). To investigate the spin structure at the interface and its effect on the origin of asymmetric field dependent EB and coercivity spin relaxation effect, isothermal remanent magnetization (IRM), thermoremanence magnetization (TRM) and training effect measurements were carried out. These measurements give insight of the complex spin structure at the core-shell interface which results into asymmetric exchange bias.

3.   Experimental results

3.1. Temperature dependent exchange bias

The magnetization (M) versus temperature (T) behaviour is plotted in Figure 2 (a). Inset figures shows the dM/dT versus log-scale -T plots, which show clear transitions at ~22 K and ~60K which are the Néel temperature (T_N) of AFM $Ni(OH)_2$ [32,33] and the blocking temperature (T_B) of super-paramagnetic Ni nanoparticles respectively. This has also been confirmed by AC susceptibility measurements. In the Figure 2c hysteresis loops of CEB at different temperatures are shown where the region near the origin is blown up. The EB, was found only below Néel temperature (T_N) of $Ni(OH)_2$ (Grey areas of Figure 2b). Below T_N the H_E, M_R, H_C and H_S rapidly increases with the decrease of temperature. The overall magnetic properties of this core-shell system is determined by the competition and combination of superparamagnetic Ni core and antiferromagnetic $Ni(OH)_2$ shell. Since below T_N both Ni and $Ni(OH)_2$ becomes ferromagnetic, the saturation field (Hs), coercivity (Hc), etc. changes rapidly as temperature decreases further below T_N. Increase of M_R below T_N indicates strong antiferromagnetic behaviour of $Ni(OH)_2$. The significant increase of H_S with the decrease of temperature is due to superparamagnetic Ni nanoparticles. At high temperature ($>T_B$) the Ni core behaves as superparamagnetic and the magnetic saturation of core-shell particles tends to originate from the AFM $Ni(OH)_2$ shell. In contrast, at low temperature ($<T_B$) the Ni core behaves as ferromagnetic which results into the sudden jump in the magnetic saturation

characteristics. The extent of CEB of core-shell nanoparticles turns out to be dependent on the field applied during field cooling and also on the path followed in tracing the loop i.e. positive or negative protocol. $|-H_{Ep}|=24$ Oe is greater than $|+H_{En}|=7$Oe, where H_{Ep} and H_{En} are for positive and negative loop tracing paths and bias fields respectively. The H_C also depends on the loop tracing protocol where for positive 50 kOe bias field (+FC) $H_{Cp}=75$ Oe and for negative 50 kOe bias field (-FC), $H_{Cn}=44$ Oe, whereas the H_C for zero-bias-field (ZFC) $H_C=63$ Oe (Figure 2d).

3.2. AC susceptibility

From the AC measurements the real χ' and imaginary χ'' parts of susceptibility for different frequencies are plotted as the function of temperature in Figure 3a and 3b respectively. Two peaks were clearly observed for each of the AC susceptibility measurements. The first peak position at low temperature remains constant at ~22 K for all frequencies which confirm the Néel temperature (T_N) of $Ni(OH)_2$ at ~22K. The position of second peak temperature around blocking temperature $(T_B \sim 60$ K) shifts towards higher temperature in frequency dependent susceptibility measurements which are expected for single-domain Ni nanoparticles. The shift of peak position (Figure 3a), observed in the real parts of susceptibility (χ') linearly increases with $\ln(\omega/2\pi)$ with the increase of frequencies (Figure 3c), which is a clear signature of SSG behaviour [34]. The proportionality constant frequency sensitivity K of T_f has been calculated to be 3.67 where T_f is peak temperature for each frequency. This frequency dependence of T_f, associated with real parts (χ') of the susceptibility follows the Vogel-Fulcher pattern (Figure 3c) which necessarily means the conventional slowing down of spin dynamics at the interface and results in the irreversibility in the SSG [31, 35-37]. Since the core-shell structure follows Vogel-Fulcher pattern, as the temperature decreases below Néel temperature the SSG at the interface freezes. As a result of that, an irreversible anisotropy is created at the core-shell interfaces. The magnitude of this irreversible anisotropy behaves differently for ascending and descending brunches of hysteresis loops and results in asymmetry in the observed exchange anisotropy. Such dynamic response of a single-domain magnetic nanoparticles ensemble can be described by the thermally-assisted magnetic relaxation process of a single-domain magnetic moment over the magnetic anisotropy energy barrier E_a [33]. The relaxation time τ associated with this dynamic response is given by a Néel–Arrhenius law $\tau = \tau_0 \exp(E_a/k_B T)$ where τ_0 is generally in the range of 10^{-9} to 10^{-11} s for SPM nanoparticles assembly [38]. The peak temperatures shift linearly with the increase of frequency following the Néel–Arrhenius equation, as shown in the χ'' measurement (Figure 3d) which is due to the dynamic response of super spins at the interface.

3.3. Spin relaxation under high field

In order to trace the origin of field dependent EB and coercivity, we investigated the spin structure of core-shell interface by well-designed spin relaxation effect measurements. The magnetic spin relaxation was studied at 2 K over a time span of 3×36000s under both +50 and −50 kOe fields. The sample was first cooled down from 350 to 2 K under zero field and then field +50 kOe, -50 kOe and +50 kOe was applied in sequence. Time dependence of the moment was measured for 36000 s for each field applied. The results of these three measurements are plotted in Figure 4a. This time dependent magnetic relaxation process clearly shows the existence of a SSG structure at the interface of FM-core and AFM-shell

[31]. A downward creep in magnetization over time signifies the incoherent rotation of the ferromagnetic moment because of the presence of SSG at the interface of the core-shell structure where and the anisotropy generated from the SSG is opposite to the applied field. The variation in moments ($|M|$) within the relaxation time (36000 sec) is almost same for alternating fields (+50 kOe/-50 kOe) which indicates the uniaxiality (UA) in FM Ni cores and its symmetric reversal for the alternating field [31]. Thus it is envisaged that the asymmetric behaviour between the descending and ascending loops could originate only from the AFM $Ni(OH)_2$ shell where the EB coupling via SSG are meant to be frozen at low temperature.

3.4. IRM & TRM

To further confirm SSG structure we carried out IRM and TRM at 2 K temperature. For the TRM measurement, the sample was cooled down from 300 K to 2 K under different fields and then the fields were removed. The remanent magnetizations (M_R) for different fields were measured immediately. The IRM was measured following zero field cooling where the sample was brought down to 2 K from 350 K under zero field and momentarily fields of different magnitudes were applied. Then the fields were removed and the remanent magnetizations (M_R) were immediately measured. Systems with SSG strongly depends on the protocol and nontrivial H-T-phase diagrams show a characteristic difference between TRM and IRM measurements [35]. The field dependence of both the IRM and TRM at 2 K are plotted in Figure 4b where both the curves rapidly increase at low field and then remain almost unchanged with further field increases which confirms the existence of SSG. Since the AFM layer is very thin (~5 nm), magnetic dilution only occurs at the interface and it is not influenced by the volume part of the AFM. No 'diluted AFM in a field (DAFF)' like behaviour could be present as in previously reported asymmetric exchange biased systems, while only SSG behaviour would exist [31, 35]. Hence, the asymmetry arises due to the formation of interfacial SSG state, which originates from disorder or defects at the interfaces of FM core and AFM shell.

3.5. Magnetic training effect

Further, the dynamics of the spin structure at the interface has been probed by studying the training effect. For training effect, CEB was measured at 2 K for 6 repeating cycles after cooling down from 350 K with +50 kOe bias field. The weakly coupled spins at the interface are realigned due to the repetitive cycle of hysteresis loop measurements, which results in the decrease of the amount of exchange bias. The dependence of H_E and H_C on the number of repeating cycles (n) is shown in Figure 5a. The H_E decreases to zero after 2 cycles and the H_C is found to be monotonically decreasing with the increase of repeating cycles. This indicates spin rearrangement at the interface which influences the EB coupling between AFM shell and FM core. It was observed that the impact of training effect is different for ascending and descending parts of the hysteresis loop which is shown in Figure 5b where loop shift is more prominent in descending part of the MH loop.

4. Discussion

The observed asymmetric loop shift visible via descending part of the hysteresis loop is conspicuous and can be explained by proposed interfacial spin freezing model. The training effect indicates that the EB is solely originated from the uncompensated frozen spins at the

interface. Both the AC susceptibility measurements (Figure 3) and magnetic spin relaxation study (Figure 4) suggest SSG behaviour at the interface. It's interesting to note that both ascending and descending curves of the hysteresis loop shrinks towards the origin of the loop due to the presence and competition of two different anisotropies where one material is relatively harder than the other. This has been previously observed in different core-shell nanoparticles systems [27, 39, 40]. In our case extra layer of SSG at the interface of superparamagnetic Ni and antiferromagnetic $Ni(OH)_2$ exists. Thus, a tri-layer-magnetic model (AFM-SSG-FM) can be proposed. In such tri-layer core-shell particles, MH loop shrinks in both descending and ascending branches during training effect measurement and the absolute value of H_{C1} decreases much faster than H_{C2}, indicating that the training behaviours at the descending and ascending branches are asymmetric (Figure 5b). Such behaviour was observed previously in other systems like NiFe/IrM [41], CoO/Co [42], BFO [31]. A significant drop in H_E between n = 1 and n = 2 is seen, and the training effect becomes insignificant when n ≥ 3. Hence the EB arises mainly due to weekly coupled FM and AFM interfacial uncompensated spins via glassy spins (SSG). The asymmetric shift in descending and ascending branches originates from the competition between long range oscillatory RKKY type coupling of spins located in the ultrathin (atomic scale) SSG layer and short range direct coupling of spins at the interface of 30 nm diameter Ni core and 5 nm thick $Ni(OH)2$ shell [43, 44]. Due to the long-range RKKY interaction in AFM/SG/FM tri-layers, the pinning spins coupled to the AFM and FM layers may extend into the entire interfacial SSG layer [45]. The training effect occurs predominantly at the first reversal of hysteresis loops where the initial cooling procedure produces metastable AFM spin structure at the interface due to the existence of SSG. Further decrease in the EB in training effect can then be considered as rearrangement of the macroscopic spin configuration toward the equilibrium. The SSG freezes at the interface either antiparallel or parallel to AFM $Ni(OH)_2$ shell depending on cooling field direction (positive and negative) which naturally leads to a pronounced change of the loop asymmetry in descending and ascending branches. Since, the EB is negative in type where FM Ni and AFM $Ni(OH)_2$ are ferromagnetically coupled via SSG and the anisotropy created at the interface by SSG is opposite to the applied field direction, the loop shift is prominent in negative field quadrant i.e. in descending branch of the loop.

Such spin glass region is a collection of spins which remains as a frozen disordered state at the interfacial region of core-shell. Hence partial random glassy state can be introduced in the Meiklejohn-Bean energy model for EB system as an effective uniaxial anisotropy [46]. Since the size of the nanoparticle core is quite big (~30nm), encapsulated by the shell of thickness ~5 nm, and the SSG is created only at the interface, the micro spin interaction at the interface below the blocking temperature can be considered as equivalent of thin films (as a first approximation). Further, the inter-particle interaction has been ignored here for the randomly oriented spherical shaped nanoparticles to simplify the angular dependent energy calculation. Hence the free energy for our system can be written as:

$E= -\mu_0 H M_F t_F \cos(\theta - \beta) - \mu_0 H M_{AF} t_{AF} \cos(\theta - \alpha) + k_F t_F \sin^2(\beta) + k_{AF} t_{AF} \sin^2(\alpha) + k_G t_G \sin^2(\beta - \alpha) - J_{RKKY}\{S_F S_G \cos\beta + S_{AF} S_G \cos\alpha\}$ ………………………..Eqn.1

where H is the external magnetic field which makes an angle θ with respect to the field cooling direction; M_F and M_{AF} are saturation magnetizations of FM and AFM part; (t_F, t_{AF}, t_G) and (k_F, k_{AF}, k_G) are the thicknesses and anisotropy constants of the FM, AFM and SSG layer

respectively; β and α are the angles between the external magnetic field and the FM/AFM moments respectively; J_{RKKY} defines the exchange coupling strength between the spins in the interface, which have magnetization of S_F, S_{AF} and S_G for respective layers. To reveal the phenomenological origin of asymmetric loop shift during training effect in such AFM/SG/FM tri-layers, we further consider Binek's model to introduce time dependence [47]. It is assumed that the asymmetric EB training effect is essentially generated from the evolution of pinning of SSG which interacts with both FM and AFM layers during magnetic cycles and contribute to EB coupling between FM Ni and AFM Ni(OH)$_2$ layers. Using Binek's model the time dependent pinning of SSG magnetization can be expressed as $S_G(t)$ because the time interval between consecutive MH loops measurement was negligible. Hence, the change of free energy F can be written as

$$\Delta F = \frac{1}{2} a \delta S_G^2(t) + \frac{1}{4} b \delta S_G^4(t) + O\left(\delta S_G^6(t)\right) \dots\dots\dots\dots\dots Eqn. 2$$

Where, the change of pinning SSG magnetization can be defined as $\delta S_G(t) = S_G(t) - S_G(\infty)$, $S_G(\infty)$ denotes final equilibrium pinning magnetization after training; a and b are arbitrary constants.

Again the evolution of pinning by SSG magnetization during the relaxation of the system towards equilibrium are determined by Landau-Khalatnikov (LK) equation [48]:

$$\xi \dot{S}_G(t) = - \frac{\partial \Delta F}{\partial S_G(t)} \dots\dots\dots\dots Eqn. 3$$

where, ξ is a phenomenological damping constant and $\dot{S}_G(t)$ is the time derivative of S_G.

Since the time interval τ required for each measurement is same, t is proportional to the number of cycle n, i.e. $t = n\tau$. If $|\delta S_G(t)|$ is significantly small the higher order terms in eqn. 2 can be ignored as they have an insignificant contribution. If we replace $\dot{S}_G(t)$ by $<dS_G/dt>$ the equation 3 is converted to difference equation. Hence, by integrating the equation 3, the cycle dependence of $S_G(n)$ for ascending (a) and descending (d) branch can be written as [49, 50]:

$$S_G^{a(d)}(n) = S_G^{a(d)}(\infty) \pm \sqrt{\frac{\xi^{a(d)}}{2b\tau}} \left(n + n_0^{a(d)}\right)^{-1/2} \dots\dots\dots\dots\dots Eqn. 4$$

where, n_0 is the initial state of the system. The signs '$\pm$' represent the increased or decreased amount of S_G during the evolution of pinning SSG magnetization.

Using the above expression for SSG in equation 1, the values of H_C obtained from the energy minimization condition can be written as:

$$H_C(n) = H_C(\infty) + k_c(n + n_0)^{-1/2} \dots\dots\dots\dots..Eqn. 5$$

It appears that the equation 5 does not fit (Figure 5a; fitting parameters as: $H_C(\infty)=19$ Oe, $k_c=11$ Oe, $n_0 = -1.3$) well with n dependency of $H_C(n)$ (where, $H_C(n) = - (H_{C1}(n) + H_{C1}(n))$ respectively. But, it fits perfectly well with n dependency of $H_{C1}(n)$ (fitting parameters as: $H_{C1}(\infty)=-15.43$ Oe, $k_{c1}=-21.9$ Oe, $n_0=-0.93$) and of $H_{C2}(n)$ (fitting parameters as: $H_{C2}(\infty)=-17.5$ Oe, $k_{c2}=13.9$ Oe, $n_0=-0.81$) independently (Figure 5b). Hence, it is clear that the modified Binek's model is not applicable for exchange-bias-shift (H_E or H_C), but applicable when loop shift in ascending and descending parts are considered separately. Hence, an asymmetric evolution in pinning of SSG magnetization exists at the interface which

distinguishes the two branches of the hysteresis loop. It is significant that k_{c1} is significantly larger than k_{c2} and opposite in sign whereas k_{c2} is nearly equal with the similar sign to k_c. Since, $|k| \propto \sqrt{\xi}$, (from equation 4 & 5) the ascending loop reacts faster compared to descending loop during the magnetic cycle as a result of frozen SSG at the core-shell interface. Depending on the bias field (positive or negative) the SSG between FM and AFM layers increased or decreased, which is depicted in equation 4. Therefore the shift in loop tracing is significantly prominent in ascending part. For the minimization of the system energy, $\delta E/\delta\alpha$ and $\delta E/\delta\beta$ must be zero and solutions for possible states (magnetic spin alignment) can be described by eight approximate solutions $\theta=0/\pi$, $\alpha=0/\pi$ and $\beta=0/\pi$. From the derived solutions it's observed that $\delta E/\delta\alpha,\beta = \delta E/\delta\alpha,\beta$ apart from $\delta E/\delta\alpha|_{\alpha=0} = -\delta E/\delta\alpha|_{\alpha=\pi}$ for $\theta=0$ [51]. Hence, the asymmetric AFM spin reversal at the interface where the EB coupling is opposite for descending loop, results into the asymmetric shift in EB loop depending on the loop tracing protocol. Such asymmetric shift in EB loop can play a critical role in the spin based electronics, i.e., spin valves, magnetic tunnel junctions, etc. Moreover, since the extent of EB is asymmetric which offers tuneablity, for instance, by adjusting suitably the extent/direction of applied field, it is possible to tune the bipolar switching of the EB, may be useful for designing appropriate protocol for writing, reading, and erasing of the next generation memory devices.

5.   Conclusions

In summary, we have successfully demonstrated the asymmetric shift of EB in Ni-Ni(OH)$_2$ core-shell nanoparticles. The loop shift has been observed only in the descending branch of the hysteresis loop. Such asymmetric shift originates due to the presence of SSG interfacial layer between AFM shell/FM core and pinning of SSG magnetization during field reversal. The spin structure at the interface of core-shell plays an important role for such asymmetric EB which can be manipulated by the diameter of the core and the thickness of the shell. The proposed multi-spin model can explain such asymmetric exchange bias behaviour of other systems as well. This is an important step forward for the understanding of EB mechanism in core-shell nanoparticles and significance of H_C in the loop shifts (H_E) of any EB system, which may underpin the development of further exchange biased applications such as single nanoparticle data storage systems, next generation memory devices, applications in medical diagnostics, magnetic resonance imaging, etc. [17, 52, 53].
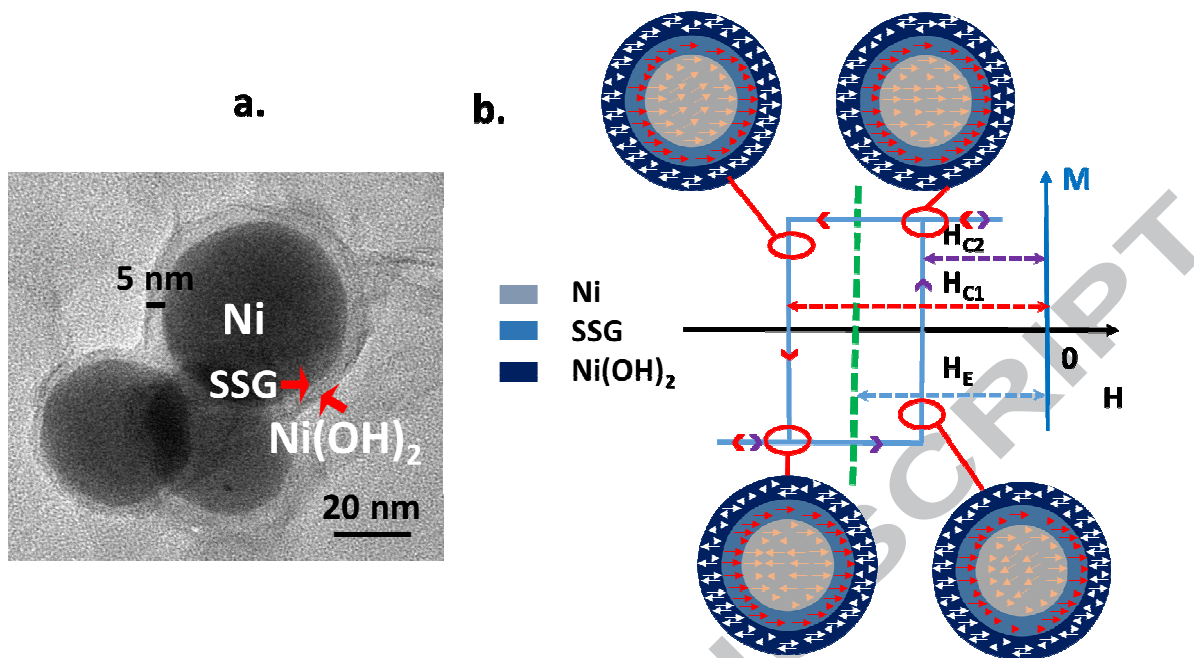
Figure 1. (a) A representative bright field TEM image of the core-shell Ni-Ni(OH)$_2$ nanoparticle. The average diameter of Ni nanoparticle size is ~30 nm and the shell thickness is ~5nm. (b) Relative orientations of the atomic moments in the FM-SSG-AFM parts. The magnitude of the EB field H_E and coercive field $H_{C1/2}$ for ascending and descending loops are defined in the figure.
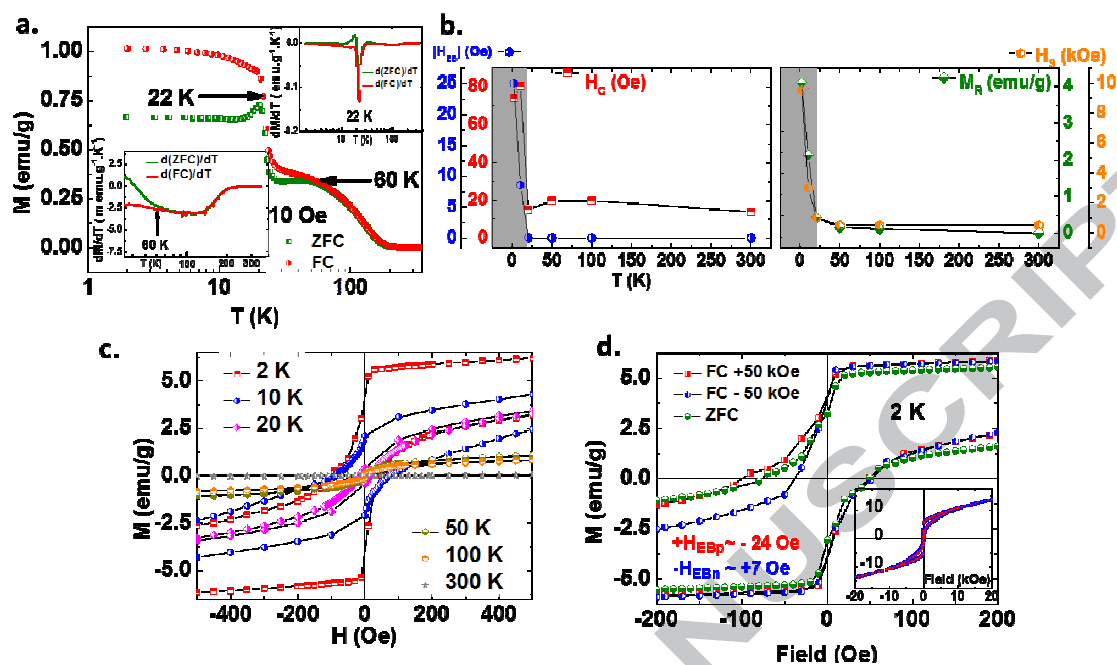
Figure 2. (a) The zero-field cooled (ZFC) and field-cooled (FC) versus temperature (T) plots (log scale); inset shows the dM/dT vs T plots to identify two transition temperature 22 K and 60 K. (b) The temperature dependence of exchange bias (H_E), coercivity (H_C), remanence magnetization (M_R), saturation magnetic field (H_S) are shown. (c) EB loop shift measured at different temperatures. (d) Conventional exchange bias (CEB) measurements at 2K. It is clearly observed the only descending part of the hysteresis loops are shifted for both positive and negative bias field. Inset figure shows the complete hysteresis loops.
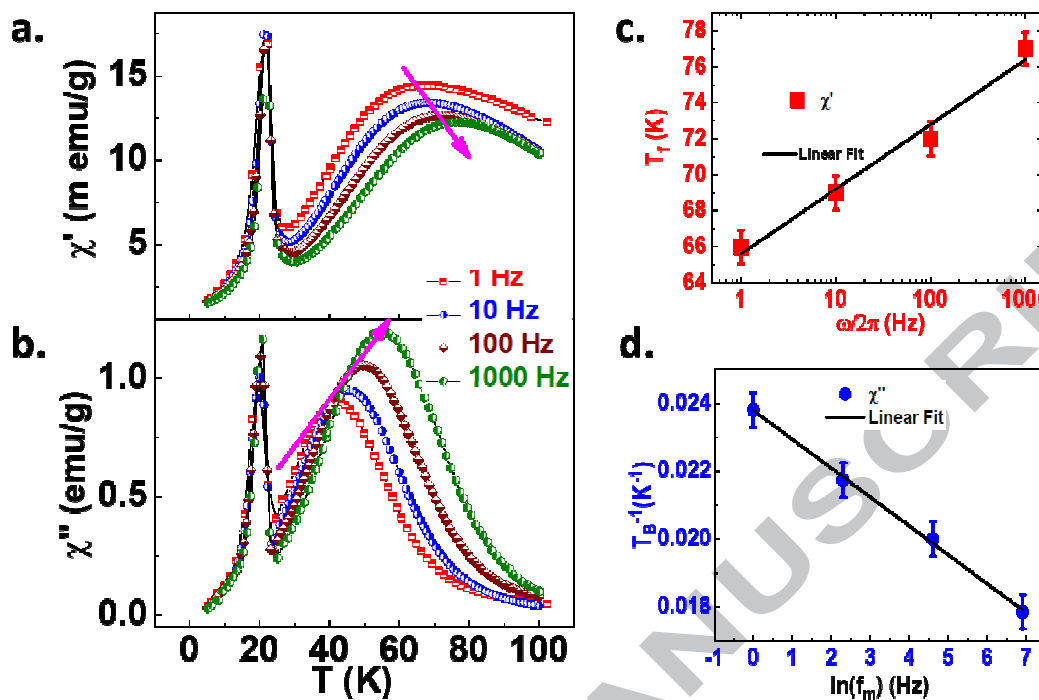
Figure 3. The real (a) and imaginary (b) ac susceptibility vs temperature (T) plot at different frequencies where the peak temperature shifts with the frequency. (c & d) The Vogel-Fulcher dependence depicting spin-glass behaviour has been observed in real χ' parts of susceptibility (red colour/square). Néel–Arrhenius model fitting to the blocking temperatures (T_B) obtained from the χ'' dataset peaks (blue colour/circle). f_m is the measured frequency. The error bar is the standard deviation of the measurement data.
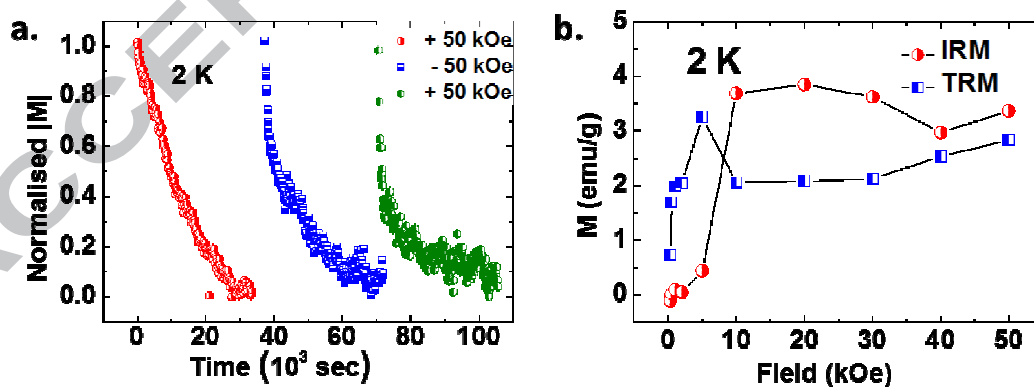
Figure 4. (a) The relaxation of the magnetization measured alternatively under +50 and −50 kOe at 2 K for 36000 seconds each; (b) field dependence of the thermo remanence (TRM) and isothermal remanence (IRM) at 2 K.
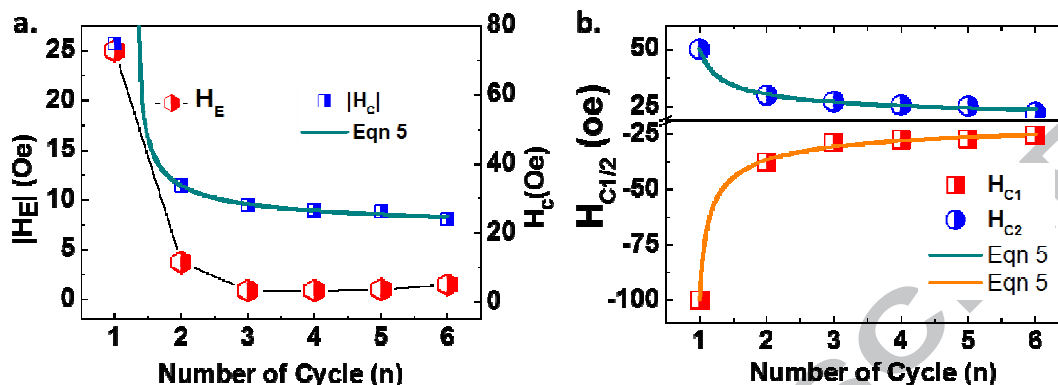
Figure 5. (a) The impact of training effect on CEB measured at 2K temperature after cooling down with +50 kOe bias field. The H_{EB} and H_C decreases with the increase in the number of hysteresis cycles (n). (b) The individual impact of training effect on descending (H_{C1}) and ascending (H_{C2}) branches are shown. The equation 5 does not fit with H_C but fits well with $H_{C1/2}$ individually.

Present address:

[3] *Department of Materials Science and Metallurgy, University of Cambridge, U.K.*

References:

1. R. H. Kodama; J. Magn. Magn. Mater. 200 (1999), 359–372

2. J. I. Martín, J. Nogués, K. Liu, J. L. Vicent, I. K. Schuller; J. Magn. Magn. Mater. 256 (2003), 449–501

3. S. Sun, C. B. Murray, D. Weller, L. Folks, A. Moser; Science 287 (2000), 1989–1992

4. U. Ha¨feli, W. Schu¨tt, J. Teller & M. Zborowski; Plenum, p. 607, New York (1997)

5. S. Chikazumi; Oxford Univ. Press, New York (1997).

6. D. Weller & A. Moser; IEEE Trans. Magn. 35 (1999), 4423–4439.

7. D. A. Thompson & J. S. Best, IBM J. Res. Dev. 44 (2000), 311–322

8. R. F. L. Evans, R. Yanes, O. Mryasov, R. W. Chantrell and O. Chubykalo-Fesenko; Europhys. Lett. 88 (2009), 57004

9. V. Skumryev, S. Stoyanov, Y. Zhang, G. Hadjipanayis, D. Givord & J. Nogués; Nature 423 (2003), 850-853

10. O. Iglesias, A. Labarta, and X. Batlle; J. Nanosci. Nanotechnol. 8 (2008), 2761.

11. J. Nogues, J. Sort, V. Langlais, V. Skumryev, S. Surinach, J. S. Munoz, and M. D. Bar; Phys. Rep. 422 (2005), 65

12. D. Tobia, E. De Biasi, M. Granada, H. E. Troiani, G. Zampieri, E. Winkler, and R. D. Zyslerless; Journal of Applied Physics 108 (2010), 104303.

13. K. Simeonidis, C. Martinez-Boubeta, O. Iglesias, A. Cabot, M. Angelakeris, S. Mourdikoudis, I. Tsiaoussis, A. Delimitis, C. Dendrinou-Samara, and O. Kalogirou; Phys. Rev. B 84 (2011), 144430.

14. X. L. Sun, N. F. Huls, A. Sigdel, and S. S. Sun; Nano Lett. 12 (2012), 246

15. H. Khurshid, W. F. Li, M. H. Phan, P. Mukherjee, G. C. Hadjipanayis, and H. Srikanth; Appl. Phys. Lett. 101(2) (2012), 022403.

16. B. Dieny, V. S. Speriosu, S. Parkin, B. A. Gurney, D. R. Wilhoit, D. Mauri; Phys. Rev. B, 43 (1991), 1297−1300.

17. C. Binns; Nanostructured Materials for Magnetoelectronics; Aktas,B., Mikailzade, F., Eds.; Springer: New York, 2013; Chapter 8.

18. Y. Hu, Y. Liu, and A. Du, J. Appl. Phys. 108(3) (2010), 033904.

19. Z. Nemati, H. Khurshid, J. Alonso, M. H. Phan, P. Mukherjee and H. Srikanth, Nanotechnology 26 (2015), 405705.

20. Y. Hu and A. Du; Phys. Status Solidi B 246, No. 10 (2009), 2384–2391.

21. P. Kumar, G. Singh, W. R Glomm, D. Peddis, E. Wahlström and R. Mathieu; Materials Research Express, 1 (2014), 036103

22. H. Khurshid, P. Lampen-Kelley, Ò. Iglesias, J. Alonso, M. Phan, C. Sun, M. Saboungi & H. Srikanth; Scientific Reports 5, (2015) Article number: 15054

23. A. N. Dobrynin, D. N. Ievlev, K. Temst, P. Lievens, J. Margueritat, J. Gonzalo, C. N. Afonso, S. Q. Zhou, A. Vantomme, E. Piscopiello, and G. Van Tendeloo; Appl. Phys. Lett. 87(1) (2005), 012501.

24. J. Nogués, V. Skumryev, J. Sort, S. Stoyanov, and D. Givord; Phys. Rev. Lett. 97 (2006), 157203

25. Teresa A.P. Rocha-Santos; Trends in Analytical Chemistry 62, 28–36 (2014)

26. Q. A. Pankhurst, N. T. K. Thanh, S K Jones and J. Dobson; J. Phys. D: Appl. Phys. 42 (2009) 224001 (15pp)

27. A. Rostamnejadi1, M. Venkatesan, P. Kameli, H. Salamati and J. M. D. Coey; J. Appl. Phys. 116 (2014), 043913

28. J. Nogués, D. Lederman, T. J. Moran, and I. K. Schuller; Phys. Rev. Lett. 76 (1996), 4624.

29. C. Leighton, J. Nogués, B. J. Jönsson-Åkerman, and Ivan K. Schuller; Phys. Rev. Lett. 84 (2000), 3466

30. T Bala, R. D. Gunning, M. Venkatesan, J. F. Godsell, S. Roy and K. M. Ryan; Nanotechnology 20 (2009), 415603

31. T Maity, S Goswami, D Bhattacharya, and S Roy; Phys. Rev. Lett. 110 (2013), 107201; Phys. Rev. B 89 (2014), 140411(R)

32. T. Takada, Y. Bando, M. Kiyama, H. Miyamoto and T. Sato; J. Phys. Soc. Jpn. 21 (1966), pp. 2745-2746

33. T. Enoki, and I. Tsujikawa; J. Phys. Soc. Jpn. 45 (1978), pp. 1515-1519

34. G. F. Goya, F. C. Fonseca, R. F. Jardim, R. Muccillo, N. L. V. Carreno, E. Longo, and E. R. Leite; J. Appl. Phys. 93(10) (2003), 6531–6533

35. J. A. Mydosh; J. Magn. Magn. Mater. 606 (1996) 157-158,

36. K. De, M. Thakur, A. Manna, and S. Giri; J. Appl. Phys. 99 (2006), 013908

37. J. L. Tholence and R. Tournier; J. Phys. (Paris), Colloq. 35 (1974), C4-229

38. G. Xiao, S.H. Liou, A. Levy, J.N. Taylor, C.L. Chien; Phys. Rev. B 34 (1986), 7573

39. D. Srikala, V. N. Singh, B. R. Mehta and S. Patnaika; J. Magn. Magn. Mater. 324 (2012), 2512–2518

40. X. Sun, N. F. Huls, A. Sigdel, and S. Sun; Nano Lett., 12 (1) (2012), pp 246–251

41. S. K. Mishra, F. Radu, H. A. Du¨rr, and W. Eberhardt; Phys. Rev. Lett. 102 (2009), 177208

42. D. L. Peng, K. Sumiyama, T. Hihara, S. Yamamuro, and T. J. Konno; Phys. Rev. B 61 (2000), 3103

43. M. Ali, P. Adie, C. H. Marrows, D. Greig, B. J. Hickey and R. L. Stamps; Nat. Mater. 6 (2007), 70

44. F. T. Yuan, J. K. Lin, Y. D. Yao and S. F. Lee; Appl. Phys. Lett. 96 (2010), 162502

45. J. A. Mydosh; Spin Glasses: An Experimental Introduction p. 105, Taylor & Francis Press (1993)

46. W. H. Meiklejohn and C. P. Bean; Phys. Rev. 102 (1956), 1413.

47. C. Binek; Phys. Rev. B 70 (2004), 014421

48. W. Kleemann; Int. J. Mod. Phys. B 7, 2469 (1993)

49. G. Vizdrik, S. Ducharme, V. M. Fridkin and S. G. Yudin; (2003) Phys. Rev. B 68 094113

50. H. Eugene Stanley, (1971), Introduction to Phase Transitions and Critical Phenomena (Clarendon Press, Oxford,), pp. 280 ff.

51. T. Maity, D. Kepaptsoglou, M. Schmidt, Q. Ramasse, S. Roy; (2017) Physical Review B 95 (10), 100401

52. J. S. Mooder, J. Nassar & G. Mathon; Annu. Rev. Mater. Sci. 29(1999), 381–432

53. M, Barbic & A. Scherer; Solid State Nucl. Magn. Reson. 28 (2005), 91–105.